

Article

Solar-Energy-Driven Cu-ZnO/TiO₂ Nanocomposite Photocatalyst for the Rapid Degradation of Congo Red Azo Dye

Vividha Kondba Landge¹, Chao-Ming Huang^{2,*}, Vikas Sadashiv Hakke¹, Shirish Hari Sonawane^{1,*}, Sivakumar Manickam³ and Ming-Chun Hsieh⁴

¹ Department of Chemical Engineering, National Institute of Technology, Warangal 506004, India; vividha12@gmail.com (V.K.L.); hakke.vikas@gmail.com (V.S.H.)

² Green Energy Technology Research Center, Department of Materials Engineering, Kun Shan University, Tainan 710, Taiwan

³ Petroleum and Chemical Engineering, Faculty of Engineering, Universiti Teknologi Brunei, Bandar Seri Begawan BE1410, Brunei; manickam.sivakumar@utb.edu.bn

⁴ Department of Materials Engineering, Kun Shan University, Tainan 710, Taiwan; michelhsieh@gmail.com

* Correspondence: charming@mail.ksu.edu.tw (C.-M.H.); shirish@nitw.ac.in (S.H.S.); Tel.: +91-8702468626 (S.H.S.)

Abstract: This study effectively demonstrates the sonochemical synthesis of visible-light-responsive Cu-ZnO/TiO₂ ternary Z-scheme heterojunction nanocomposite photocatalyst. The as-prepared photocatalyst was comprehensively characterized by techniques including high-resolution transmission electron microscopy (HRTEM), field emission scanning electron microscopy (FE-SEM) with energy dispersive X-ray analysis (EDX) and elemental dot mapping, X-ray diffraction (XRD), UV-Vis-diffuse reflectance spectroscopy (UV-Vis-DRS), Brunauer–Emmett–Teller (BET) surface area, and Fourier-transform infrared spectroscopy (FTIR). The photocatalytic activity of the Cu-ZnO/TiO₂ nanocomposite photocatalyst was assessed for the degradation of Congo red (CR), an azo dye, under direct sunlight. The pseudo-first-order rate constant for CR degradation was found to be 0.09 min⁻¹. The outcome implies that the synthesised nanocomposite photocatalyst demonstrates excellent photocatalytic activity under direct sunlight as 98% degradation of CR dye was achieved in approximately 20 min using the Cu-ZnO/TiO₂ nanocomposite photocatalyst. Furthermore, its high recoverability and reusability of five times indicate its excellent catalytic potential.

Keywords: Cu-ZnO/TiO₂; nanocomposite; dye degradation; Congo red; photocatalysis; ultrasound; sonochemical; energy; Z-scheme heterojunction



Citation: Landge, V.K.; Huang, C.-M.; Hakke, V.S.; Sonawane, S.H.; Manickam, S.; Hsieh, M.-C. Solar-Energy-Driven Cu-ZnO/TiO₂ Nanocomposite Photocatalyst for the Rapid Degradation of Congo Red Azo Dye. *Catalysts* **2022**, *12*, 605. <https://doi.org/10.3390/catal12060605>

Academic Editor: Detlef W. Bahnemann

Received: 7 April 2022

Accepted: 31 May 2022

Published: 2 June 2022

Publisher's Note: MDPI stays neutral with regard to jurisdictional claims in published maps and institutional affiliations.



Copyright: © 2022 by the authors. Licensee MDPI, Basel, Switzerland. This article is an open access article distributed under the terms and conditions of the Creative Commons Attribution (CC BY) license (<https://creativecommons.org/licenses/by/4.0/>).

1. Introduction

Water pollution from numerous sectors is currently a major concern worldwide [1]. As a result, environmental preservation and water purification are the most critical criteria for conserving natural water resources necessary for advancing the world [2]. Contaminants can be found in wastewater from various industries and municipal and agricultural sources. The type of contaminants in the wastewater determines the best treatment technology criteria. Organic and inorganic recalcitrant pollutants such as azo dyes, phenolic compounds, and heavy metals are commonly found in industrial wastewaters [3]. The recalcitrant pollutants have been detrimental to humans and aquatic life due to their non-biodegradability, high toxicity, and carcinogenic consequences. As a result, a major concern among researchers is their removal/degradation before discharge from the industry. Congo red (CR) (disodium 4-amino-3-[4-[4-(1-amino-4-sulfonato-naphthalen-2-yl)diazenyl]phenyl]phenyl]diazenyl-naphthalene-1-sulfonate), an azo dye, is a recalcitrant contaminant that is exceedingly difficult to decompose [3].

Advanced oxidation process (AOP) is one of the most successful strategies for removing colors from wastewater [4]. It is cost-effective, highly efficient, requires low energy consumption, operates under mild conditions, presents broad applicability, and reduces

secondary pollution. AOPs are both destructive and low-/no-waste-producing solutions for the remediation of contaminated water. Contaminants and their intermediates can be mineralised by AOPs [5]. Recently, a great surge in interest in harnessing solar energy as a clean and sustainable energy source for the photodegradation of recalcitrant contaminants has been noticed [6]. It can immediately transform recalcitrant contaminants into safer compounds in wastewater to gain the research community's interest.

Photocatalytic processes initiate upon the illumination of the light with photons having higher energy than the band gap energy of semiconductor material, causing the motion of electrons from the valence band (VB) to the conduction band (CB). Adsorbed substrates are oxidised, and active oxygen species are reduced by a hole–electron pair formed when the CB receives an electron from the VB, leaving behind a hole. Adsorbed water or hydroxide ions in an aqueous solution are oxidised by holes in the VB, forming hydroxyl radicals, whilst molecular oxygen is reduced by the electrons in the CB and forms semiconductor superoxide radicals. Organic pollutants, such as dyes, are oxidised by hydroxyl and superoxide radicals and disintegrate into carbon dioxide and water [7].

TiO₂ and ZnO nanoparticles (NPs) exhibiting wide-band-gap energies of 3.2 eV and 3.37 eV are capable materials for water treatment applications. They are inexpensive, non-toxic, and provide high surface area [8]. One drawback of TiO₂ and ZnO as photocatalysts is that they have a large band gap, which can only be activated by ultraviolet irradiation. Due to this, several investigations have been conducted to either adjust the band gap energy of these semiconductor metal oxides or find alternatives to harness solar energy. To increase solar light sensitivity, many techniques are exploited, including (a) doping with other elements and (b) creation of heterojunction structures by mixing semiconductors with metals or other semiconductors [9,10].

Based on this, intense research is focused on improving the light-harvesting capacity and stability of TiO₂ and ZnO NPs by doping them with noble and non-noble metals. For example, Ag-ZnO [11], Cu-ZnO [12], ZnO-Sm [13], sulphated TiO₂-WO₃ [14], TiO₂-GO [15], Gd-ZnO [16], TiO₂-ZnO [17–20], Fe-TiO₂ and Ce-TiO₂ [21] have been reported for the photocatalytic applications. These heterojunction nanocomposite materials showed enhancement in photocatalytic activity compared to the individual nanomaterials. They have greater light-harvesting abilities and lower charge carrier recombination rates due to adequate surface imperfections and band alignment [13,17,22]. Among the most studied heterojunctions, TiO₂-ZnO type-II heterojunctions have received immense interest because of the synergic effects caused by the introduction of electrons to TiO₂ from the conduction band of ZnO, which reduces the electron–hole recombination [19,20,23–25]. However, it should be emphasised that the majority of the studies were carried out under UV radiation, suggesting that the TiO₂/ZnO lattice may still be employed effectively for visible light photocatalysis [26].

Recent studies have explored doping of various noble, non-noble transition metals as an electron mediator (EM) onto the TiO₂-ZnO heterojunction to improve the catalytic performance under visible light through the formation of Z-scheme heterojunction [8,22,27]. Liang et al. demonstrated the effectiveness of ternary TiO₂-ZnO/Au nanocomposite over TiO₂, TiO₂-Au and TiO₂-ZnO for photocatalytic hydrogen production under visible-light illumination coupling of ZnO and TiO₂ and the localised surface plasmonic resonance of Au NPs [8]. However, the incorporation of noble metals is not cost-effective. Cu, on the other hand, is now employed as a competent dopant for several visible-light-responsive photocatalysts, exhibiting redox potentials as low as 0.52 V (Cu²⁺/Cu) and 0.16 V (Cu²⁺/Cu⁺) [28,29]. Cu presents a low-band-gap energy (1.98–2.02 eV), is non-toxic, is chemically stable, possesses good thermal and electrical conductivities, is abundant, and is environmentally friendly, leading to its widespread employment in various applications. Even though adding a dopant to the ZnO/TiO₂ heterojunction may enhance its physical and chemical characteristics, only a few studies have looked into this aspect, which necessitates this investigation.

This is the first work focusing on impregnating Cu and ZnO NPs onto TiO₂ to form Cu-ZnO/TiO₂ ternary Z-scheme heterojunction nanocomposite photocatalyst to enhance the photocatalytic decomposition of CR azo dye under natural sunlight. We demonstrate a facile one-pot method to synthesise Cu-ZnO/TiO₂ nanocomposites via the sonochemical co-reduction method. The novelty involved in this work is the synthesis of heterogeneous visible-light-activated photocatalyst and its performance in dye degradation as well as reusability. The outcome of this study provides a roadmap to developing highly efficient nanocomposite photocatalysts for wastewater treatment and remediation with numerous synergies.

2. Results

2.1. Structural, Morphological, and Optical Characterization of Cu-ZnO/TiO₂ Nanocomposite Photocatalyst

A facile and rapid sonochemical approach facilitated the one-pot synthesis of the Cu-ZnO/TiO₂ nanocomposite photocatalyst. The Cu-ZnO/TiO₂ nanocomposite photocatalyst with various wt% of Cu, ZnO and TiO₂ named as CZT-1 (wt% = Cu-0; ZnO-40; TiO₂-60), CZT-2 (wt% = Cu-10; ZnO-30; TiO₂-60), CZT-3 (wt% = Cu-20; ZnO-20; TiO₂-60), CZT-5 (wt% = Cu-30; ZnO-10; TiO₂-60), CZT-5 (wt% = Cu-40; ZnO-0; TiO₂-60) was synthesized. For comparison, pure Cu and pure ZnO catalysts were also synthesised using the sonochemical approach. Furthermore, a detailed characterization was conducted for the sample CZT-2 nanocomposite photocatalyst. The crystalline structure and average crystallite size were obtained through an XRD pattern. The XRD analysis was carried out at 10° to 100° at room temperature with Cu K α radiation. The obtained XRD for the CZT-2 nanocomposite photocatalyst, pure Cu, pure ZnO, and pure TiO₂ is presented in Figure 1. It could be observed that the characteristic diffraction peaks for individual Cu, ZnO, and TiO₂ shown in Figure 1 coincide with the peaks of the CZT-2 nanocomposite photocatalyst and are indexed accordingly in Figure 1a. This confirms the presence of crystalline Cu and ZnO on the TiO₂ surface in the synthesized nanocomposite. The sharp diffraction peaks observed at 31.80°, 34.52°, 36.46°, 47.63°, 56.58°, and 62.97° in Figure 1a are attributed to (100), (002), (101), (102), (110), and (103) planes of the hexagonal crystalline structure of wurtzite ZnO. These results align with the JCPDS Card no. 36-1451 [30], while Cu displayed FCC structure in the CZT-2 nanocomposite photocatalyst as (111), (200), (220), (311), and (222); planes were observed at 2 θ = 43.34°, 50.52°, 74.2°, 89.90°, 95.22°, respectively, in Figure 1a and are indexed according to JCPDS card no. 04-0836 [31]. The XRD pattern also reveals the presence of mixed anatase and rutile phases of TiO₂ in the prepared nanocomposite as the characteristics peaks for rutile TiO₂ were observed at 36.46° (101), 43.34° (210), 56.58° (220), 62.97° (002) [JCPDS card no. 21-1276] along with anatase TiO₂ observed at 47.63°, 67.93°, and 74.20° corresponding to (200), (116), and (215) planes [JCPDS card no. 21-1272], respectively [18,32,33]. Figure 1d shows the XRD pattern for anatase TiO₂ according to JCPDS card no. 21-1272. While Figure 1a reveals the presence of both phases of TiO₂. The possible reason for the presence of both anatase and rutile phases of TiO₂ in the Cu-ZnO/TiO₂ nanocomposite photocatalyst could be the acoustic cavitation employed for the synthesis of Cu-ZnO/TiO₂ nanocomposite, as the local hot spots generated during cavitation can facilitate the transformation of anatase to rutile phase owing to the high temperature and pressure conditions possessed by the local cavities. Munguti and Dejene [18] and Chen et al. [34] have also reported the transformation of anatase TiO₂ to rutile TiO₂ as a result of high temperature employed during the synthesis of nanocomposite.

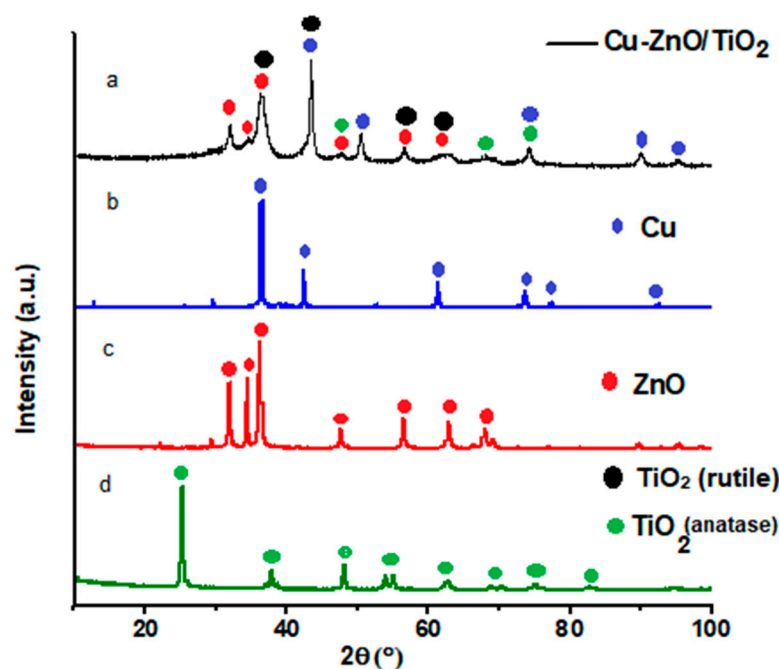


Figure 1. XRD pattern of the sonochemically synthesised Cu-ZnO/TiO₂ (CZT-2) nanocomposite photocatalyst (a) Cu (b) ZnO (c) and TiO₂ (d) nanoparticles.

Using a sonochemical technique, the efficient production of CZT-2 nanocomposite photocatalyst is confirmed as the presented XRD pattern is entirely attributed to Cu, TiO₂, and ZnO (Figure 1a). For the high-intensity peak at 43.34°, the Debye–Scherrer equation (Equation (1)) was used to compute the average crystallite size of the CZT-2 nanocomposite.

$$d = k\lambda / \beta \cos\theta \quad (1)$$

where d is the average crystallite size, k is the particle shape factor (0.94), λ is the wavelength (1.5406 Å), β is the full width at half maximum (0.368) of the high-intensity diffraction peak, and θ is the Bragg's angle. Using the Debye–Scherrer equation, the average crystallite size of the obtained CZT-2 nanocomposite was 24.27 nm. Furthermore, using the Debye–Scherrer equation, the crystallite sizes of pure Cu, ZnO, and TiO₂ were estimated as 2 nm, 43 nm, and 36.9 nm, respectively. The CZT-2 nanocomposite synthesised via the sonochemical approach shows a highly crystalline structure and uniform particle size.

The morphological characteristics of the CZT-2 nanocomposite photocatalyst were studied using FESEM analysis (Figure 2a). The as-prepared nanocomposites display spherical morphology with an approximately uniform size of 25 nm, as evident through the FESEM micrograph, supporting the size calculations obtained through XRD analysis (24.27 nm). The distribution and composition of Cu-ZnO NPs over TiO₂ were investigated using FESEM-EDX and elemental dot mapping analysis, as shown in Figure 2b,c, respectively. The FESEM-EDX micrograph (Figure 2b) of the CZT-2 nanocomposite reveals the sharp peaks of Cu, Zn, O, and Ti elements only, assuring the existence of Cu, ZnO, and TiO₂ in the nanocomposite photocatalyst.

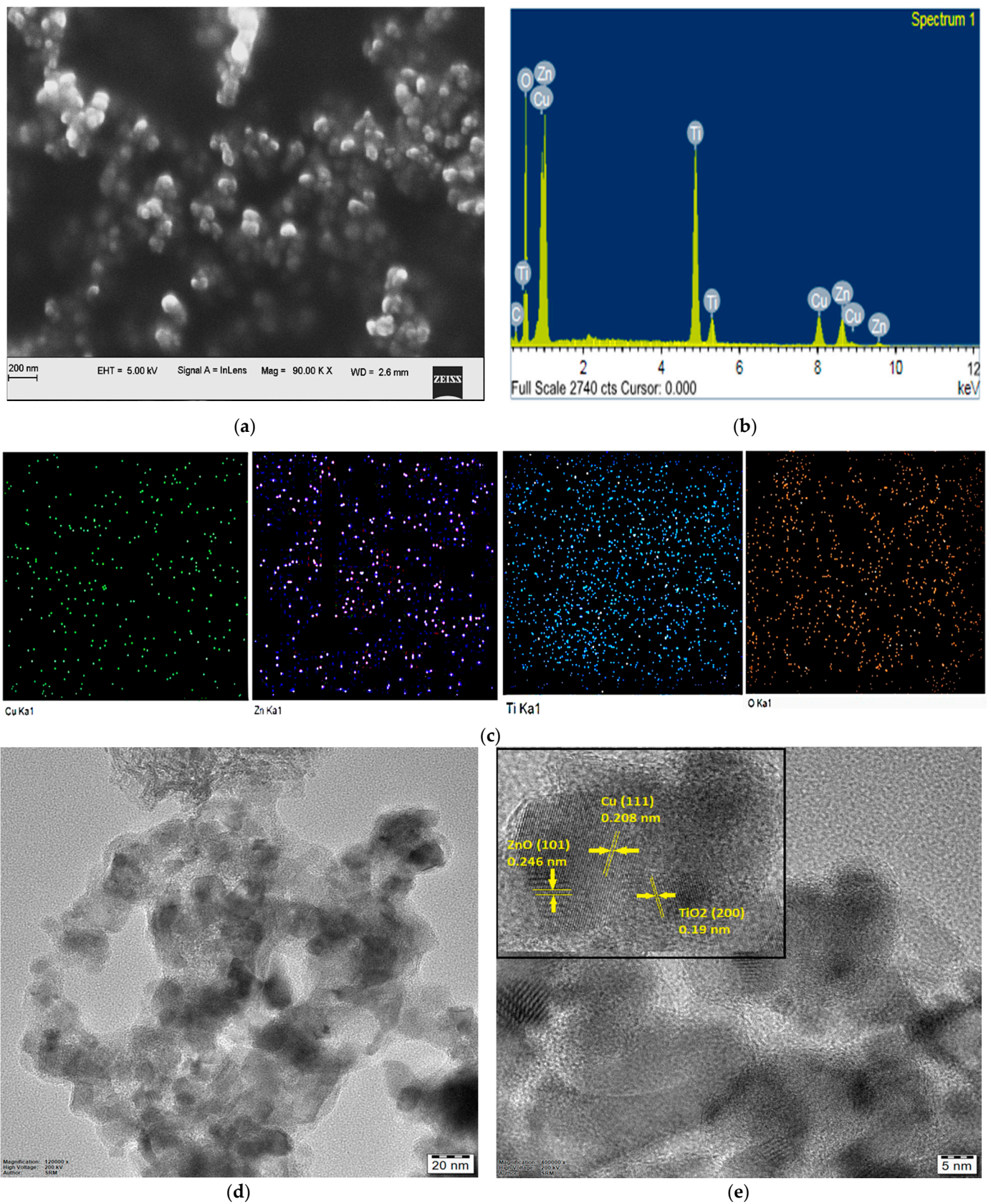


Figure 2. (a) FESEM image (b) EDX (c) Elemental mapping images (d,e) HRTEM images of Cu-ZnO/TiO₂ (CZT-2) nanocomposite photocatalyst.

In contrast, the peak corresponding to the C element arises due to the carbon tape used during EDX analysis. Table 1 lists the photocatalyst components and their wt%, with TiO₂ being the most abundant, followed by ZnO and Cu. The FESEM-EDX elemental dot mapping images (Figure 2c) illustrate the elemental dot distribution in the CZT-2 nanocomposite photocatalyst. Overall, the uniform anchoring of Cu, Zn, Ti, and O was detected from the dot mapping of the constituent elements of the as-prepared nanocomposite photocatalyst, implying the achievement of even dispersion of Zn and Cu over the TiO₂ surface. This proves that the uniformity in shape, size, and distribution of dopant materials over the support surface is demonstrated through the co-reduction of Cu and Zn metal precursors over TiO₂ NPs assisted by ultrasound.

Table 1. Elemental composition of Cu-ZnO/TiO₂ (CZT-2) nanocomposite photocatalyst on weight basis.

Nanocomposite	Cu (wt%)	Zn (wt%)	O (wt%)	Ti (wt%)	C (wt%)
Cu-ZnO/TiO ₂	9.67	13.05	48.84	18.27	10.17

Furthermore, the detailed morphological characteristics of CZT-2 were assessed by HRTEM images, as shown in Figure 2d,e. Figure 2d reveals that the as-synthesised nanocomposite photocatalyst displays a nearly spherical shape with the average nanoparticle size comparable to the crystallite size, which was deduced using the Debye–Scherrer equation. The uniform deposition of Cu and ZnO over TiO₂ without aggregation can also be observed in Figure 2d. The HRTEM micrographs reveal the distinct lattice fringes indicating the formation of polycrystalline CZT-2 nanocomposites. As the TiO₂ and ZnO possess nearly the same characteristics, these semiconductors do not reflect any differences in the HRTEM images, as shown in Figure 2d. However, the dark-coloured particles represent Cu present on light-shaded TiO₂ and ZnO. Although TiO₂ and ZnO cannot be distinguished clearly through the HRTEM images, the lattice spacings of ca. 0.208 nm, 0.246 nm, and 0.19 nm belong to the diffraction planes of Cu (111), wurtzite ZnO (101), and anatase TiO₂ (200), respectively (Figure 2e). Thus, Figure 2e proves the co-existence of Cu and ZnO over TiO₂ and confirms the formation of a ternary CZT-2 nanocomposite with Z-scheme heterojunction. In addition, the presence of Cu, ZnO, and TiO₂ was established through FESEM-EDX and elemental dot mapping analysis.

Notably, CZT-2 nanocomposite fabrication exhibited uniform spherical Cu and Zn metal NPs with the particle size of the composite being about 25 nm and even distribution of Cu and ZnO over the TiO₂ surface is achieved successfully through the sonochemical approach.

The functional groups attached to the CZT-2 nanocomposite photocatalyst were determined through the FTIR analysis conducted from 4000 to 400 cm⁻¹. The resultant FTIR spectrum for the CZT-2 nanocomposite photocatalyst is depicted in Figure 3. The characteristic peaks belonging to the metal oxides' lattice vibrations were below 1500 cm⁻¹. Accordingly, the band around 449 cm⁻¹ is the distinctive peak for Zn-O stretching vibrations, while the band at 662 cm⁻¹ arises due to Cu-O stretching. The bands related to Ti-O stretching vibration and Ti-O-Ti skeleton bending vibrations could be observed at 713 and 1053 cm⁻¹, respectively [22,23]. The symmetric and asymmetric stretching vibrations of Zn-O-Zn are observed through the intense peak at 1378 cm⁻¹ [22]. The adsorbed moisture over the CZT-2 surface gives rise to the bending and stretching vibrations of -OH groups, as seen through the bands at 1628 and 3446 cm⁻¹, respectively [35]. The band appearing at 2335 cm⁻¹ is attributed to the adsorbed atmospheric CO₂, whereas at 2918 cm⁻¹ indicates C-H stretching [18]. Hence, FTIR confirms the facile synthesis of CZT-2 via a sonochemical approach through the co-existence of Cu, ZnO, and TiO₂ as their characteristic bands are revealed at 449, 622, 713, 1053, and 1378 cm⁻¹.

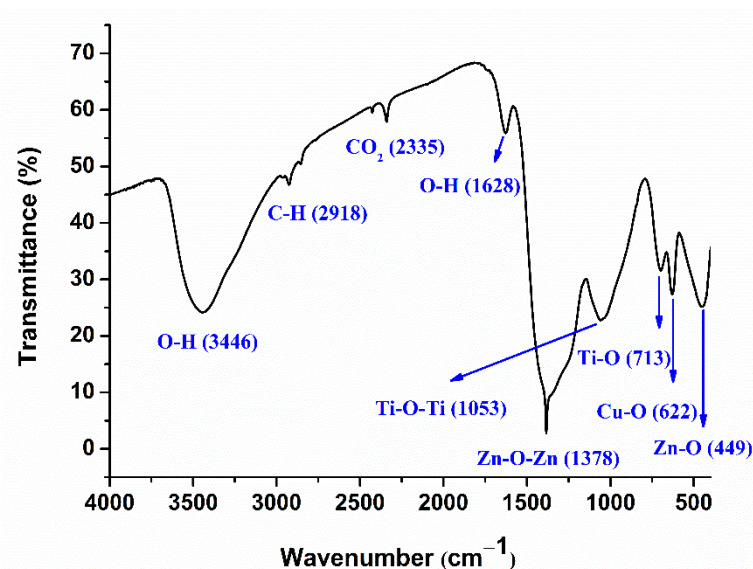


Figure 3. FTIR of the Cu-ZnO/TiO₂ (CZT-2) nanocomposite photocatalyst.

The BET surface area of CZT-2 evaluated from the BET surface area plot, as shown in Figure 4a,b, was estimated to be 60.52 m²/g. The external surface area and micropore volume were determined using the t-plot method and were 31.25 m²/g and 13.98 m³/g, respectively.

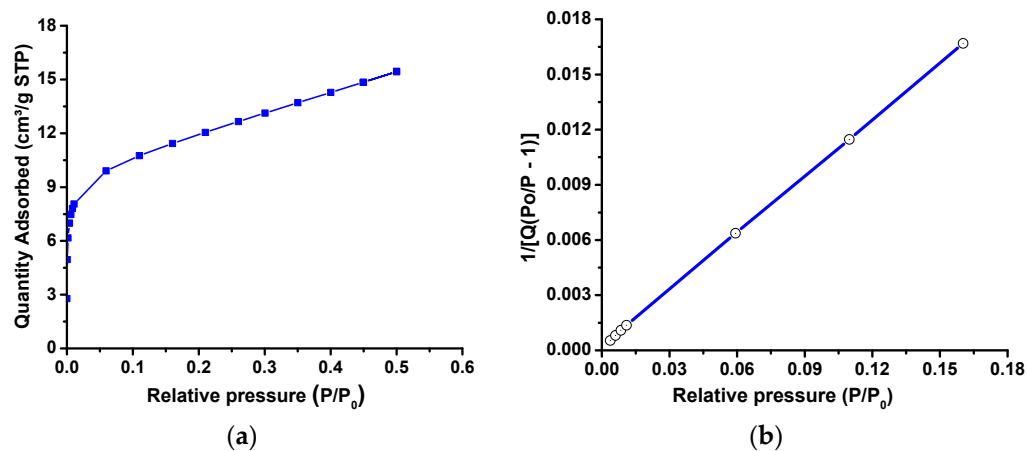


Figure 4. (a) BET isotherm linear plot (b) BET surface area plot for Cu-ZnO/TiO₂ (CZT-2) nanocomposite photocatalyst.

The optical properties of the proposed Cu-ZnO/TiO₂ nanocomposite photocatalyst were analysed to evaluate its ability to harness solar energy for photocatalytic applications. The band gap energy of the CZT-2 nanocomposite photocatalyst was estimated using UV-Vis-diffuse reflectance spectroscopy (UV-Vis-DRS), as illustrated in Figure 5. The CZT-2 nanocomposite photocatalyst can absorb the visible-light irradiation as the absorption edge was reflected around 470 nm. The improved sensitivity of CZT-2 towards visible-light irradiation can be ascribed to the oxygen vacancies created in the band gaps of ZnO and TiO₂ because of copper doping [26]. Cu acts as an electron mediator and forms a Cu-ZnO/TiO₂ Z-scheme heterojunction nanocomposite photocatalyst. As demonstrated in Figure 5, the band gap energy of the proposed nanocomposite photocatalyst was estimated from the onset of the linear increase in the diffuse reflectance spectra, as reported by Joseph et al. [36]. The diffuse reflectance spectrum of the CZT-2 reveals the linear region between 500 nm and 650, corresponding to the band edge absorption. The band gap energy

was determined by the intercept of the extrapolation of the linear fit to $R = 0$ and was 2.68 eV (Figure 5). The remarkable decrease in the band gap energy of the as-produced nanocomposite photocatalyst was observed in comparison with the band gap energies reported for the pure TiO_2 ($E_g = 3.2$ eV) [27], pure ZnO ($E_g = 3.37$ eV) [8], and ZnO- TiO_2 heterojunction ($E_g = 3.15$ eV) [23,27]. The narrow-band-gap energy of CZT-2 might result from incorporating Cu and ZnO on TiO_2 , giving rise to the synergistic effect among them during the sonochemical synthesis of the Cu-ZnO/ TiO_2 nanocomposite photocatalyst.

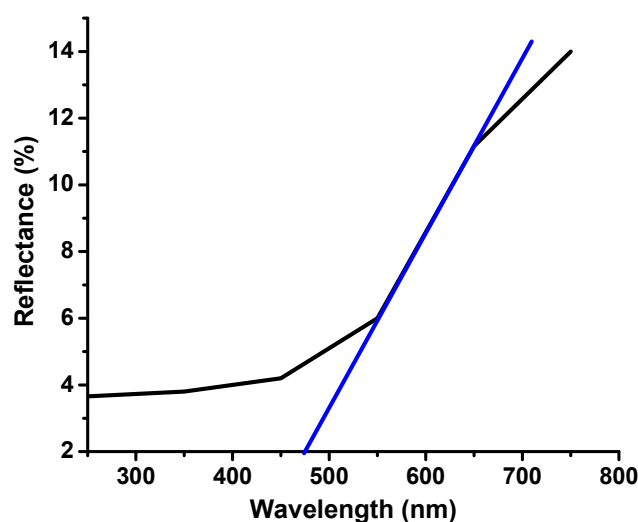


Figure 5. UV-Vis-diffuse reflectance spectra of the Cu-ZnO/ TiO_2 (CZT-2) nanocomposite photocatalyst.

2.2. Assessment of Photocatalytic Efficacy

Congo red (CR), an azo dye, is highly fatal, stable, and difficult to mineralise. Thus, CR degradation was performed to evaluate the photocatalytic efficacy of the as-synthesised Cu-ZnO/ TiO_2 nanocomposite photocatalyst using a renewable energy source, i.e., natural sunlight. Upon the direct illumination of sunlight having a higher amount of energy than the band gap energy of Cu-ZnO/ TiO_2 nanocomposite photocatalyst (2.68 eV), the electron transmission through the VB of photocatalyst to its CB occurs, which leaves a hole in the VB. This results in the generation of electron–hole pairs. Subsequently, these charges move toward the photocatalyst surface, where the electron reacts with O_2 to give superoxide ($\bullet\text{O}_2^-$) radicals while holes react with H_2O to give hydroxyl ($\bullet\text{OH}$) radicals. The produced $\bullet\text{O}_2^-$ and $\bullet\text{OH}$ radicals are highly oxidising radicals and are responsible for the degradation of adsorbed CR dye and produce H_2O , CO_2 , and other mineralisation products.

CR degradation studies were conducted under direct sunlight irradiation with and without the as-prepared nanocomposite photocatalysts. For comparison, the photocatalytic degradation of CR dye was also conducted with pure Cu, pure ZnO, and pure TiO_2 catalysts. It was observed that CR degradation does not occur in the absence of photocatalyst even after 180 min of sunlight illumination. On the contrary, the CR degradation rates were higher in the presence of synthesised nanocomposite photocatalysts, which can be ascribed to the photocatalytic degradation of the catalysts. Then, CR degradation was attempted in the presence of as-prepared photocatalysts for up to 180 min in the dark. In the absence of sunlight illumination, significant colour change or change in the absorbance of CR dye was not detected. This suggests that the CR dye decomposition cannot proceed without the photocatalyst or sunlight.

The photocatalytic CR degradation was conducted under sunlight radiation over Cu-ZnO/ TiO_2 photocatalysts. Before sunlight illumination, CR dye solution and photocatalyst were kept in the dark for about 30 min to ensure the adsorption and desorption equilibrium between the CR dye solution and photocatalyst. The UV-visible absorption spectra for the samples were recorded at fixed intervals. The absorbance for the distinctive peak of CR

dye and the colour of CR dye gradually decreased with the sunlight illumination time, as shown in Figure 6. This implies the instantaneous onset of CR degradation with sunlight illumination over the Cu-ZnO/TiO₂ (CZT-2) nanocomposite photocatalysts. However, it was observed that the nanocomposite photocatalysts revealed enhanced photocatalytic efficiency compared to pure ZnO, pure Cu, and pure TiO₂. At the same time, pure ZnO displayed higher photocatalytic activity than pure TiO₂, while pure Cu showed the least efficiency. Similar results were reported by Munguti and Dejene [18], Pragathiswaran et al. [22], and Delsouz Khaki et al. [26]. Table 2 summarises the photocatalytic efficacy of all the prepared nanocomposite samples towards photocatalytic degradation of CR. The Cu-ZnO/TiO₂ nanocomposite photocatalysts offered higher photocatalytic performance than either individual ZnO, TiO₂, or Cu catalysts. The CZT-2 sample presented the highest photodegradation efficacy with almost complete photodegradation of CR dye after 20 min. This ultrafast CR dye decomposition was obtained due to the enhanced properties emerging from the synergy among Cu, ZnO, and TiO₂ in the nanocomposite photocatalyst. Figure 6 suggests that the characteristic absorbance peak of CR dye diminishes completely along with a simultaneous decrease in the intensity of dye solution colour until it becomes colourless within 20 min of sunlight exposure over CZT-2 nanocomposite photocatalyst.

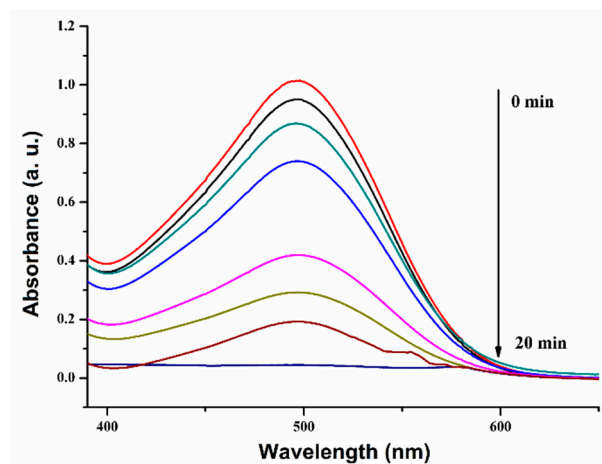


Figure 6. UV-Visible absorption spectra for the CR degradation with time over CZT-2 nanocomposite photocatalyst (reaction conditions: CR dye = 75 mg/L, catalyst loading = 0.5 g/L, sunlight irradiation = 20 min).

Table 2. Photocatalytic performance of the prepared nanocomposite photocatalysts for CR degradation (reaction conditions: CR dye = 75 mg/L, catalyst loading = 0.5 g/L).

Photocatalyst	Degradation Time (min)	K_{app} (min ⁻¹)	Degradation (%)
TiO ₂	100	0.013	76
ZnO	60	0.05	99
Cu	70	0.02	94
CZT-1	55	0.071	93
CZT-2	20	0.094	100
CZT-3	40	0.075	96
CZT-4	65	0.06	91
CZT-5	60	0.04	86
Cu-ZnO	35	0.078	96

Furthermore, the samples with lower or higher wt% of Cu and ZnO on TiO₂ in the nanocomposite led to decreased photocatalytic activity than the CZT-2 sample. The reduced photocatalytic activity of the nanocomposites with low ZnO levels could be due lack of highly catalytic ZnO in the Cu-ZnO/TiO₂ nanocomposite. The pure ZnO revealed higher photocatalytic efficacy than the Cu and TiO₂, implying that Cu and TiO₂ could dominate in the lower ratios of ZnO in the nanocomposites, plummeting its photocatalytic efficiency.

Delsouz Khaki et al. reported similar catalytic activity for methyl orange and methylene blue dye degradation over Cu doped TiO₂/ZnO photocatalyst [26]. They reported 85.45% removal of methyl orange and 73.20% removal of methylene blue over 0.6 g/L Cu-TiO₂/ZnO with an initial dye concentration of 20 ppm under visible-light illumination after 120 min. They synthesised a Cu-TiO₂/ZnO catalyst via the sol-gel method with three steps of sol preparation: drying of sol in an electric oven, calcination, and ball milling to obtain the nano-sized Cu-TiO₂/ZnO composite. The synthesis process took approximately 18–20 h and produced crystallites with an average size of 37.65 nm and rodlike shapes having lengths of 300–400 nm and 50–60 nm diameters. In this sonochemical approach, the synthesis of Cu-ZnO/TiO₂ nanocomposite photocatalyst was obtained within 45 min of sonochemical reduction followed by 6 h of drying. Moreover, an average crystallite size of 24.27 nm with spherical morphology was achieved. This suggests the superiority of the sonochemical approach for synthesising Cu-ZnO/TiO₂ nanocomposite photocatalyst over the sol-gel approach. Additionally, this insinuates the potential of as-prepared Cu-ZnO/TiO₂ nanocomposite photocatalyst for the removal of various recalcitrant dyes and phenolic compounds in wastewater streams using sunlight energy.

2.2.1. Kinetic Studies of CR Decomposition over Cu-ZnO/TiO₂ Nanocomposite Photocatalyst

UV-visible spectroscopy is useful to track CR degradation and for kinetic studies. The Beer-Lambert law states that the absorbance intensity of dye changes linearly with its concentration. Thus, the photocatalytic degradation rate of CR dye was investigated through the declining intensity of the CR characteristic peak, as illustrated in Figure 6. At the same time, the Langmuir-Hinshelwood model was employed to depict the kinetic studies between Cu-ZnO/TiO₂ nanocomposite photocatalysts and CR dye molecules. As the initial CR dye concentration (C_i) is small, the Langmuir-Hinshelwood model could be considered to follow the pseudo-first-order rate equation (Equation (2)) [9].

$$\ln \frac{C_i}{C_t} = K_{app} \cdot t \quad (2)$$

This indicates that the slope of the linear fit for $\ln(C_i/C_t)$ vs. irradiation time gives the apparent degradation rate constant (K_{app}). Figure 7 elucidates the degradation kinetics plot for CR degradation over sunlight driven Cu-ZnO/TiO₂ nanocomposite photocatalysts.

The values of K_{app} and degradation (%) for the prepared nanocomposite photocatalysts are reported in Table 2. The degradation kinetics demonstrated by the CZT-2 Z-scheme heterojunction nanocomposite photocatalyst for CR photocatalytic degradation is outstanding compared to other synthesised composite samples and other reported reports of photocatalysts for CR degradation. The K_{app} for photocatalytic CR degradation over the CZT-2 nanocomposite photocatalyst under sunlight irradiation was 0.094 min⁻¹. Magdalane et al. reported 85% CR degradation over TiO₂-doped CoFe₂O₄ under visible light after 120 min [37]. Yang et al. obtained 99.63% CR degradation over ternary metal selenide-chitosan microspheres after 2 h of sunlight irradiation [38]. Further, Huerta-Aguilar et al. achieved 64.7% CR degradation over ZnO-TiO₂ in 70 min of UV-light illumination. With a ZnO-TiO₂-Ag nanocomposite photocatalyst, 87.5 % CR degradation after 70 min of UV-light irradiation has been reported [27]. This signifies that the doping of ZnO-TiO₂ heterojunction with low-band-gap materials can greatly influence dye degradation [8,22,27]. The efficacy of several catalysts described in the literature for CR dye decomposition is exhibited in Table 3. As evident from Table 3, the nanocomposite materials reveal good pho-

photocatalytic efficiency compared to the individual materials. However, the Cu-ZnO/TiO₂ nanocomposite photocatalyst explored in this study manifested excellent efficiency towards CR removal in terms of initial CR concentration to catalyst-loading ratio, CR removal time, and K_{app} harnessing the natural sunlight. This swift removal of CR obtained in the present study can be attributed to the synergistic properties of incorporating Cu into the ZnO-TiO₂ heterojunction. Additionally, a good improvement in the photocatalyst's sunlight-driven excitation was observed due to the incorporation of Cu into the ZnO-TiO₂, resulting in the formation of a Z-scheme heterojunction. The CZT-2 nanocomposite photocatalyst presented the highest catalytic activity among other prepared nanocomposites towards CR photocatalytic degradation, confirmed through its photocatalytic performance. Thus, the catalyst characterization and further studies were conducted using the CZT-2 nanocomposite photocatalyst.

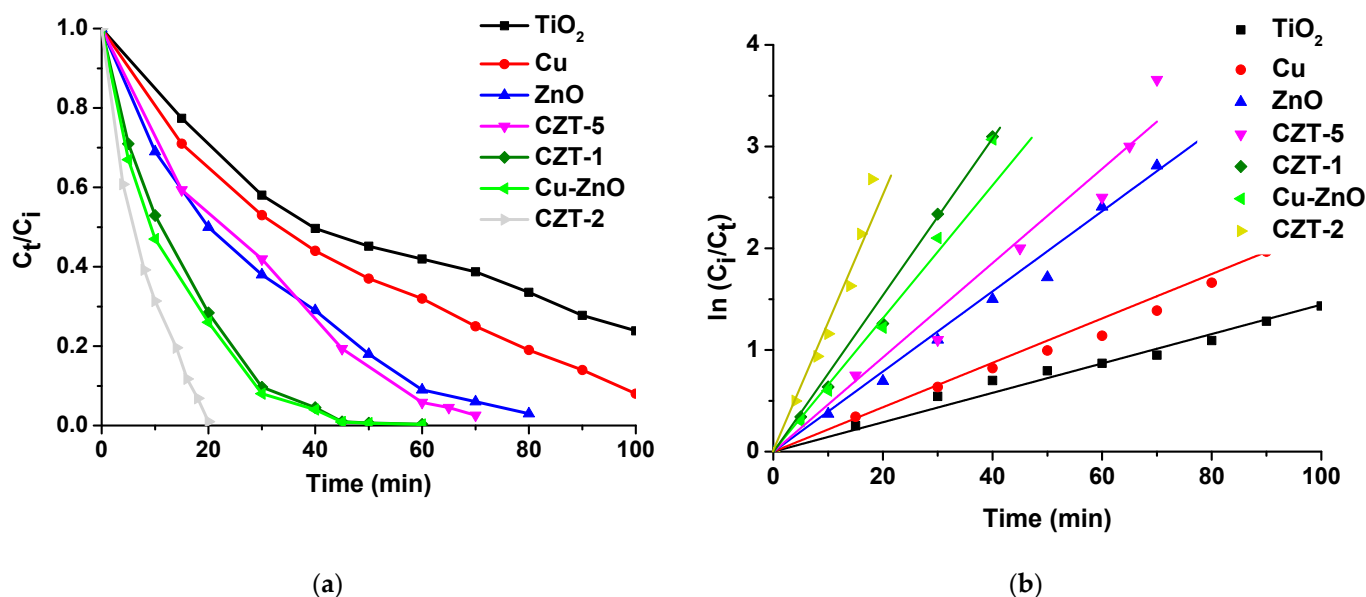


Figure 7. (a) Photocatalytic degradation of CR with different catalysts (b) The kinetic plot of CR degradation between $\ln(C_i/C_t)$ and time (t) (reaction conditions: CR dye = 75 mg/L, catalyst loading = 0.5 g/L, sunlight irradiation = 20 min).

2.2.2. Influence of Catalyst Loading, Sunlight Illumination Time, and Initial CR Concentration on the CR Degradation

The catalyst loading has a considerable impact on the abatement of CR dye, as illustrated in Figure 8a. The impact of catalyst dosage on CR decomposition was evaluated by varying the CZT-2 photocatalyst loading from 0.1 g/L to 0.8 g/L under sunlight for 20 min with 75 mg/L of CR dye concentration. As shown in Figure 8a, the CR dye removal rises as the catalyst loading increases up to 0.5 g/L. When the amount of catalyst increases, the availability of reactive sites and surface area increases, facilitating the generation of many oxidising radicals. This improves the effectiveness of CR dye decomposition up to a catalyst loading of 0.5 g/L. Conversely, a further increase in the catalyst dosage does not promote the CR dye decomposition; rather, it marginally diminishes the degradation efficiency. This occurs as the dye solution becomes more and more impenetrable to sunlight due to the increase in the catalyst dosage. As a result, the amount of visible light energy that could be adsorbed on the catalyst's surface becomes insufficient, lowering the photocatalyst's CR dye degradation efficacy [39]. These results align with the studies reported by Delsouz Khaki et al. [26] towards the photocatalytic decomposition of methyl orange and methylene blue dye over sunlight activated Cu-TiO₂/ZnO.

Table 3. Summary of the photocatalytic performance of different catalysts used for CR degradation.

Photocatalyst	Catalytic Dosage (g)	CR Concentration (mg/L)	Degradation Time (min)	K_{app} (min^{-1})	Degradation (%)	References
ZnO	0.05	16	60	0.0062	53.1	[9]
Pd-ZnO	0.05	16	60	0.0576	100	[9]
TiO ₂ doped CoFe ₂ O ₄	0.08	10	120	-	85	[37]
FeNiSe-CHM	0.2	60	140	-	99	[38]
ZBiSe-CM	0.225	40	120	0.045	99.63	[39]
ZnO/Geopolymer	0.2	5	60	0.048	96.97	[40]
g-C ₃ N ₄ /RGO/Bi ₂ Fe ₄ O ₉	0.05	10	60	0.022	86.76	[41]
PbTiO ₃ nanorods	0.75	7	150	0.017	92	[42]
MgZnCr-TiO ₂	0.05	100	40	-	98	[43]
TiO ₂	0.1	17.4	30	-	87	[44]
CuO	0.05	20	210	-	67	[45]
CuO-ZnO/Egg shell	0.1	10	240	-	83	[46]
ZnO-TiO ₂	0.1	70	70	0.0065	87.5	[27]
Cu-ZnO/TiO₂ (CZT-2)	0.025	75	20	0.094	100	Present work

The sunlight illumination time can greatly affect the CR degradation. As indicated earlier, without sunlight illumination, CR decomposition does not occur. On the contrary, beyond 15 min, the degradation rate increases gradually. Thus, the decomposition of CR dye (75 mg/L) was observed from 0 min to 20 min over the CZT-2 photocatalyst (0.5 g/L) and is reflected in Figure 8b. The increase in CR degradation efficiency with increasing sunlight illumination time was observed until it reached 100% after 20 min of sunlight illumination. Up to 15 min, a rapid increase of 78 % CR decomposition after 15 min of contact time was recorded. This might occur due to the photocatalyst surface's reactive site saturation as a high dye concentration (75 mg/L) was used for the photocatalytic decomposition studies. A similar trend in the decomposition of CR dye with time was also reported by Yang et al. [38].

Several researchers have reported that the decomposition of recalcitrant azo dyes can be significantly altered based on the initial CR dye concentration [26,38,42]. Hence, the CR removal efficiency of the as-prepared CZT-2 nanocomposite photocatalyst was investigated by changing the initial CR dye concentration from 55 mg/L to 95 mg/L with the catalyst dosage of 0.5 g/L up to 15 min. As indicated in Figure 8c, it is evident that the CR removal efficiency declines with an increase in the initial CR concentration. The CR decomposition efficiency was reduced from 88% to 60%, with the initial CR dye concentration increasing from 55 mg/L to 95 mg/L after 15 min of sunlight. This phenomenon is apparent as the increasing CR concentration increases the rate of active site saturation of the photocatalyst surface and hinders the passage of photons to reach the photocatalyst surface by blocking the path of light due to excessive CR molecules in the suspension. Such interception of sunlight radiation reduces electron-hole pair generation, significantly lowering the CR removal efficiency. This behaviour was also noted by Khan et al. [40] and Ma et al. [43].

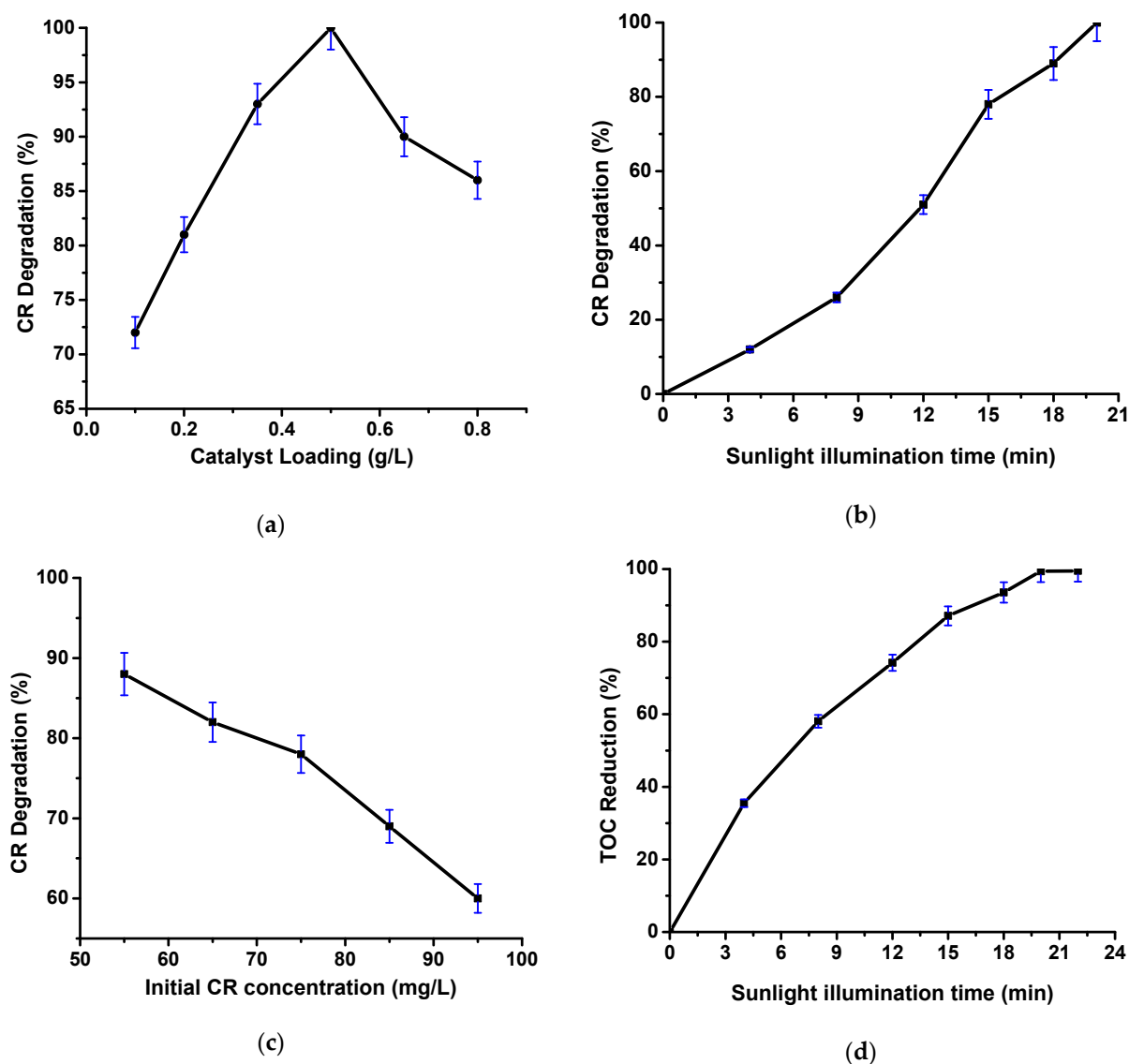


Figure 8. CR degradation efficiency with (a) Catalyst loading (b) Sunlight illumination time (c) Initial CR concentration and (d) TOC removal efficiency.

2.2.3. Assessment of TOC Abatement during Photocatalytic Degradation of CR Dye

The extent of mineralization of CR degradation (75 mg/L) was examined by analysing the TOC removal (%) with sunlight illumination time over CZT-2 nanocomposite catalyst (0.5 g/L). The TOC removal efficiency is demonstrated in Figure 8d. A drastic reduction in TOC along with time could be observed, indicating increased mineralization with time. Almost complete mineralization of CR dye was achieved after 20 min of sunlight illumination, implying complete degradation of CR dye.

2.2.4. Photocatalyst Stability

The stability and ease of recycling are the critical factors in determining the applicability of heterogeneous catalysts. Thus, the recyclability of the CZT-2 nanocomposite photocatalyst during sequential photocatalytic CR dye decomposition was investigated in this work. A fresh CR dye solution was used in every recycle run while the recycle photocatalyst was employed to conduct the recycle runs. The photocatalyst was separated and washed with DI water using a simple centrifugal operation at the end of every trial. The photocatalysts recovered were again used in a subsequent photocatalytic CR degradation process. Figure 9 depicts the nanocomposite photocatalyst's recyclability and efficacy for

CR dye degradation under sunlight illumination for five successive recycle runs. After the third run, a small drop in the catalytic activity was noticed. Overall, Cu-ZnO/TiO₂ (CZT-2) nanocomposite photocatalyst demonstrates excellent stability for CR degradation up to five recycle runs with no significant loss in the catalytic activity.

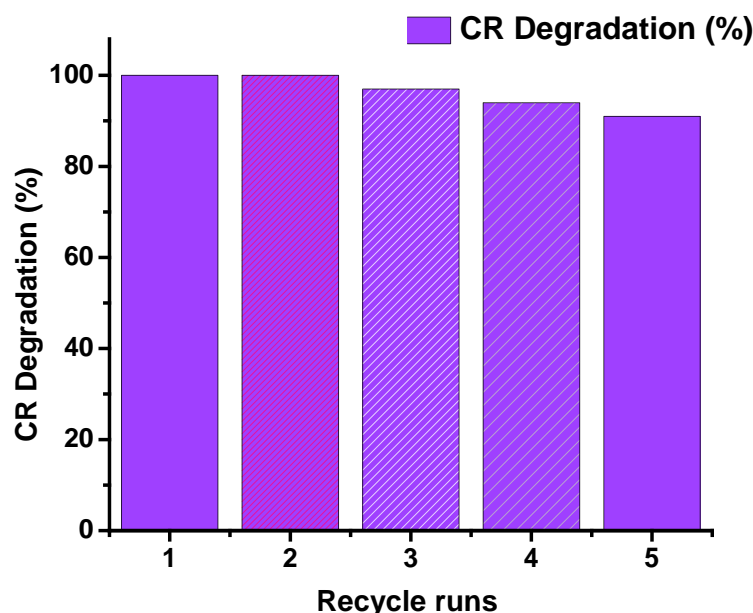


Figure 9. Reusability of Cu-ZnO/TiO₂ (CZT-2) nanocomposite photocatalyst for CR degradation (reaction conditions: CR dye = 75 mg/L, catalyst loading = 0.5 g/L, sunlight irradiation = 20 min).

2.2.5. Plausible Mechanism for the Enhanced Photocatalytic Performance of Cu-ZnO/TiO₂ Nanocomposite Photocatalyst

Generally, for TiO₂-ZnO, type II heterojunction is reported between TiO₂ and ZnO, which is well known for obtaining an efficient degradation. In the TiO₂-ZnO type II heterojunction, mostly localization of electrons occurs on TiO₂ and holes are accumulated on ZnO, which prevents the recombination of the charge carriers, enhancing the photocatalytic activity [20]. However, the electron transfer is limited by the coulomb repulsions among photo-generated electrons. To overcome this, recently, a Z-scheme system has attracted widespread attention, which is an effective construction to boost the catalytic activities of photocatalysts [47]. An EM is added between the semiconductor heterojunction in the Z-scheme heterojunction. In the proposed nanocomposite photocatalyst, Cu plays the role of an EM between ZnO and TiO₂, which accelerates the transfer of electrons in the Cu-ZnO/TiO₂, thereby greatly improving the photocatalytic activity. As a result, the band alignment of Cu-ZnO/TiO₂ heterojunction is Z-scheme (Figure 10). Based on the above discussion and reported studies [34,47], a tentative mechanism for the photocatalytic degradation of CR dye over the Cu-ZnO/TiO₂ composite has been proposed.

The photo-induced electrons are preferably transferred from CB of TiO₂ to Cu, attributing to the more positive Fermi level of Cu than CB energy of TiO₂ by the strong interfacial built-in electronic field [47]. Since the Fermi level of Cu is lower than the VB energy of ZnO, the trapped accumulated electrons in metal Cu will be partially transferred from the Fermi level of Cu to VB of ZnO, and the photo-generated holes of ZnO are quenched; hence, the photo-induced electrons of ZnO can be separated efficiently and enhance the reduction ability. Furthermore, the accumulated holes in the VB of TiO₂ will be able to oxidise the CR molecules. Owing to the reasons mentioned above, the Cu-ZnO/TiO₂ Z-scheme heterojunction exhibits an excellent photocatalytic activity. Thus, the Cu-ZnO/TiO₂ nanocomposite photocatalyst can efficiently promote photocatalytic degradation of CR dye. The possible charge transfer mechanism for the Cu-ZnO/TiO₂ nanocomposite photocatalyst towards CR dye degradation is illustrated in Figure 10.

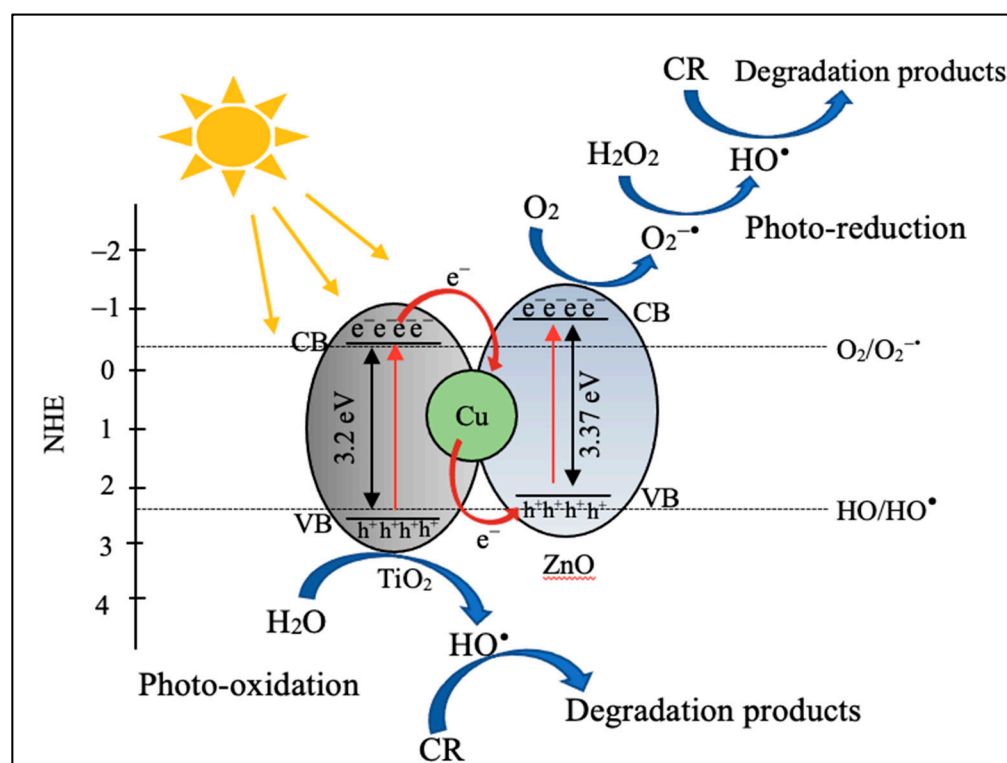


Figure 10. Charge transfer mechanism for Z-scheme Cu-ZnO/TiO₂ (CZT-2) heterojunction photocatalyst for CR degradation.

3. Materials and Methods

3.1. Reagents

As zinc precursor, zinc acetate (C₄H₆O₄Zn·2H₂O, 98.5%) (S.D. Fine Chemicals Pvt. Ltd., Chennai, India) was used. For copper, copper sulphate pentahydrate (CuSO₄·5H₂O, 98.5%) precursor from Hi-Media Laboratories Pvt. Ltd., Mumbai, India, was employed. The metals were reduced using sodium borohydride (NaBH₄, 97%) obtained from Molychem, Mumbai, India. As a stabiliser, polyvinylpyrrolidone (C₆H₉NO)_n (PVP, 11.5–12.8%, MW 40,000, Hi-Media Laboratories Pvt. Ltd., India) was used. TiO₂ NPs support was obtained from Merck Pvt. Ltd., Bengaluru, India. Sigma-Aldrich (Hyderabad, India) provided the CR dye. De-ionized (DI) water was used to obtain precursor, reducing agent, and CR dye solutions.

3.2. Sonication-Assisted Synthesis of Cu-ZnO/TiO₂ Ternary Z-Scheme Heterojunction Nanocomposite Photocatalyst

The ternary Cu-ZnO/TiO₂ nanocomposite was synthesised via the sonochemical co-reduction of CuSO₄·5H₂O and C₄H₆O₄Zn·2H₂O in the presence of TiO₂ NPs. At first, 100 mL TiO₂ NPs suspension in DI water was prepared using an ultrasound probe sonicator (20 kHz, 20 mm tip diameter, 220 W, Dakshin ultrasonicator, Mumbai, India) operated with pulse mode (5 s ON and 5 s OFF) for 10 min. To this dispersion, an appropriate quantity of CuSO₄·5H₂O, C₄H₆O₄Zn·2H₂O and PVP was added, and the solution was stirred to dissolve the metal precursors fully. These metal precursors were then reduced with dropwise addition of 0.2 M NaBH₄ (50 mL) and ultrasonic irradiation for up to 40 min using a probe sonicator operated with pulse mode (5 s ON and 5 s OFF). Centrifugation was employed to extract and wash the resulting nanocomposite with DI water. The washed precipitate was then dried at 80 °C for 6 h to provide the ternary Cu-ZnO/TiO₂ nanocomposite photocatalyst. The Cu-ZnO/TiO₂ nanocomposite photocatalyst with various wt% of Cu, ZnO and TiO₂ named as CZT-1 (wt% = Cu-0; ZnO-40; TiO₂-60), CZT-2 (wt% = Cu-10; ZnO-30; TiO₂-60), CZT-3 (wt% = Cu-20; ZnO-20; TiO₂-60), CZT-5 (wt% = Cu-30; ZnO-10;

TiO₂-60), CZT-5 (wt% = Cu-40; ZnO-0; TiO₂-60) was synthesized. For comparison, pure Cu and pure ZnO catalysts were also synthesised using the sonochemical approach.

3.3. Characterization of the As-Prepared Cu-ZnO/TiO₂ Z-Scheme Heterojunction Nanocomposite Photocatalyst

Fourier-transform infrared spectroscopy (FTIR) was carried out to check the functional groups bound to the surface of the as-prepared photocatalyst. The compact Fourier-transform infrared spectrometer of Bruker-ALPHA II with a resolution of 4 cm⁻¹ between 4000 cm⁻¹ and 400 cm⁻¹ was utilised to record the FTIR. The crystal structure, phase detection and average crystallite size estimation of Cu-ZnO/TiO₂ were conducted using the X-ray diffractogram (XRD) of the obtained Cu-ZnO/TiO₂. The XRD was performed using a Malvern Panalytical X-ray diffractometer with CuKα radiation (1.5406 Å). The morphological aspects were studied with a high-resolution transmission electron microscope (HRTEM) (JEOL-JEM 2100, Tokyo, Japan) operated at 200 kV and the overall distribution of Cu, ZnO, and TiO₂ in the as-prepared nanocomposite was investigated with Carl Zeiss, EVO MA 15 (Oxford Instruments, Abingdon, UK) field emission scanning electron microscope (FESEM) equipped with energy-dispersive X-ray spectroscopy (EDX). The optical properties of Cu-ZnO/TiO₂ were examined via UV-Vis-DRS conducted on Specord 210 Plus UV-Vis spectrophotometer (Analytikjena, Jena, Germany). The surface area measurement was performed on Micromeritics ASAP 2020 BET analyser. Over time, the degradation of CR dye was observed via a double-beam UV-visible spectrophotometer (UV 2080 UV-visible spectrophotometer, Analytical Technologies Limited, Vadodara, India). The extent of CR dye mineralisation was investigated using a total organic carbon (TOC) analyser (TOC-L_{CPN} analyser, Shimadzu, Kyoto, Japan).

3.4. Photocatalytic Performance of the Sunlight-Driven CR Dye Degradation over Cu-ZnO/TiO₂

The photocatalytic efficiency of ternary Cu-ZnO/TiO₂ heterojunction nanocomposite catalyst was investigated to degrade CR dye as a model pollutant. To a 50 mL CR dye solution (75 mg/L), 0.5 g/L Cu-ZnO/TiO₂ nanocomposite catalyst was added and maintained in the dark for up to 30 min with continuous stirring to establish the adsorption equilibrium. CR dye solution with catalyst was then subjected to direct sunlight illumination under constant stirring. The decrease in the concentration of CR with time was noted by recording the UV-visible absorbance of the reaction samples at regular intervals. The samples were collected at regular intervals, followed by catalyst separation using a centrifuge before UV-visible absorbance measurements. The CR degradation was computed using Equation (3).

$$\text{CR degradation (\%)} = \frac{C_i - C_t}{C_i} \times 100 = \frac{A_i - A_t}{A_i} \times 100 \quad (3)$$

where C_i is the initial concentration of CR, A_i is the initial absorbance of the CR dye, C_t is the concentration of CR at time t , and A_t is the absorbance of CR dye after sunlight illumination at time t .

After the complete CR decomposition, the catalyst was extracted using a centrifuge, washed and dried. The stability of the catalyst was investigated by repeating the same photocatalytic experiment using the recovered catalyst for five cycles consecutively, and the respective CR degradation was noted.

4. Conclusions

In this study, a Cu-ZnO/TiO₂ Z-scheme heterojunction nanocomposite photocatalyst was synthesised using the sonochemical approach. The average crystallite size of the CZT-2 nanocomposite photocatalyst was 24.27 nm, as determined through XRD. In comparison, uniformity in shape and size with spherical morphology was illustrated through HRTEM and FESEM analyses. The CZT-2 nanocomposite revealed high visible-light absorption capability as it showed a narrow-band-gap energy of 2.68 eV. The photocatalytic activity of the Cu-ZnO/TiO₂ nanocomposite was evaluated for sunlight-driven photocatalytic CR

dye decomposition. The CZT-2 photocatalyst revealed excellent photocatalytic efficacy as 100% CR decomposition with complete mineralisation was attained after only 20 min of sunlight irradiation. The pseudo-first-order reaction kinetics were applied to estimate the K_{app} for CR decomposition over the Cu-ZnO/TiO₂ photocatalyst. Rapid degradation of CR was observed over the CZT-2 nanocomposite photocatalyst with $K_{app} = 0.094 \text{ min}^{-1}$. This enhancement in the photocatalytic activity was noted due to the excellent characteristics and catalytic properties offered by the synergy between Cu, ZnO, and TiO₂ present in the ternary Z-scheme heterojunction nanocomposite. Furthermore, the photocatalyst stability was studied for five successive recycle runs. The solar-light-responsive photocatalyst showed outstanding stability up to five recycle runs with no apparent loss in the catalytic performance. This implies that the nanocomposite photocatalyst synthesised via the sonochemical approach can find its applications in wastewater treatment for photocatalytic degradation of various dyes, phenolic compounds, and other difficult-to-treat compounds. Furthermore, utilising this solar-light-responsive photocatalyst can also offer the scale-up potential for treating textile wastewaters in bulk.

Author Contributions: V.K.L. contributed to designing methodology, conducting formal analysis, investigation, data curation, and writing the original draft of the manuscript; V.S.H. contributed to the investigation and data analysis; S.H.S. conceptualised the work along with supervising, resourcing, administration of work, and reviewing the draft; S.M. contributed to data analysis, thorough reviewing, writing, and editing of the manuscript; C.-M.H. and M.-C.H. contributed to project administration and funding acquisition. All authors have read and agreed to the published version of the manuscript.

Funding: This research was funded by the Science and Engineering Research Board of the Government of India, grant number EMR/2016/007585, and The APC was supported by Green Energy Technology Research Center from The Featured Areas Research Center Program within the framework of the Higher Education Sprout Project by the Ministry of Education (MOE) in Taiwan.

Conflicts of Interest: The authors declare no conflict of interest.

References

1. Thomas, M.; Naikoo, G.; Sheikh, M.U.D.; Bano, M.; Khan, F. Effective photocatalytic degradation of Congo red dye using alginate/carboxymethyl cellulose/TiO₂ nanocomposite hydrogel under direct sunlight irradiation. *J. Photochem. Photobiol. A Chem.* **2016**, *327*, 33–43. [[CrossRef](#)]
2. Moradzadeh, A.; Mahjoub, A.; Sadjadi, M.S.; Sadr, M.H.; Farhadyar, N. Investigation on synthesis, characterization and photocatalytic degradation of congo red by Zn-doped CdTiO₃/TiO₂. *Polyhedron* **2019**, *170*, 404–411. [[CrossRef](#)]
3. Pathania, D.; Gupta, D.; Al-Muhtaseb, A.; Sharma, G.; Kumar, A.; Naushad, M.; Ahamad, T.; Alshehri, S.M. Photocatalytic degradation of highly toxic dyes using chitosan-g-poly(acrylamide)/ZnS in presence of solar irradiation. *J. Photochem. Photobiol. A Chem.* **2016**, *329*, 61–68. [[CrossRef](#)]
4. Cako, E.; Gunasekaran, K.D.; Soltani, R.D.C.; Boczkaj, G. Ultrafast degradation of brilliant cresyl blue under hydrodynamic cavitation based advanced oxidation processes (AOPs). *Water Resour. Ind.* **2020**, *24*, 100134. [[CrossRef](#)]
5. Patil, S.P.; Bethi, B.; Sonawane, G.; Shrivastava, V.; Sonawane, S. Efficient adsorption and photocatalytic degradation of Rhodamine B dye over Bi₂O₃-bentonite nanocomposites: A kinetic study. *J. Ind. Eng. Chem.* **2016**, *34*, 356–363. [[CrossRef](#)]
6. Habibi, M.H.; Rahmati, M.H. The effect of operational parameters on the photocatalytic degradation of Congo red organic dye using ZnO–CdS core–shell nano-structure coated on glass by Doctor Blade method. *Spectrochim. Acta Part A Mol. Biomol. Spectrosc.* **2015**, *137*, 160–164. [[CrossRef](#)]
7. Khairrol, N.F.; Sapawe, N.; Danish, M. Excellent Performance Integrated both Adsorption and Photocatalytic Reaction toward Degradation of Congo Red by CuO/Eggshell. *Mater. Today Proc.* **2019**, *19*, 1340–1345. [[CrossRef](#)]
8. Liang, Y.; Li, W.; Wang, X.; Zhou, R.; Ding, H. TiO₂-ZnO/Au ternary heterojunction nanocomposite: Excellent antibacterial property and visible-light photocatalytic hydrogen production efficiency. *Ceram. Int.* **2021**, *48*, 2826–2832. [[CrossRef](#)]
9. Güy, N.; Çakar, S.; Özacar, M. Comparison of palladium/zinc oxide photocatalysts prepared by different palladium doping methods for congo red degradation. *J. Colloid Interface Sci.* **2016**, *466*, 128–137. [[CrossRef](#)]
10. Gong, E.; Ali, S.; Hiragond, C.B.; Kim, H.S.; Powar, N.S.; Kim, D.; Kim, H.; In, S.-I. Solar fuels: Research and development strategies to accelerate photocatalytic CO₂ conversion into hydrocarbon fuels. *Energy Environ. Sci.* **2022**, *15*, 880–937. [[CrossRef](#)]
11. Motshekg, S.C.; Ray, S.S.; Onyango, M.S.; Momba, M. Microwave-assisted synthesis, characterization and antibacterial activity of Ag/ZnO nanoparticles supported bentonite clay. *J. Hazard. Mater.* **2013**, *262*, 439–446. [[CrossRef](#)] [[PubMed](#)]

12. Salehi, K.; Daraei, H.; Teymouri, P.; Shahmoradi, B.; Maleki, A. Cu-doped ZnO nanoparticle for removal of reactive black 5: Application of artificial neural networks and multiple linear regression for modeling and optimization. *Desalination Water Treat.* **2016**, *57*, 22074–22080. [[CrossRef](#)]
13. Pascariu, P.; Cojocaru, C.; Olaru, N.; Samoila, P.; Airinei, A.; Ignat, M.; Sacarescu, L.; Timpu, D. Novel rare earth (RE-La, Er, Sm) metal doped ZnO photocatalysts for degradation of Congo-Red dye: Synthesis, characterization and kinetic studies. *J. Environ. Manag.* **2019**, *239*, 225–234. [[CrossRef](#)] [[PubMed](#)]
14. Patil, S.; Deshmukh, S.; More, K.; Shevale, V.; Mullani, S.; Dhodamani, A.; Delekar, S. Sulfated TiO₂/WO₃ nanocomposite: An efficient photocatalyst for degradation of Congo red and methyl red dyes under visible light irradiation. *Mater. Chem. Phys.* **2018**, *225*, 247–255. [[CrossRef](#)]
15. Zhang, H.; Wang, X.; Li, N.; Xia, J.; Meng, Q.; Ding, J.; Lu, J. Synthesis and characterization of TiO₂/graphene oxide nanocomposites for photoreduction of heavy metal ions in reverse osmosis concentrate. *RSC Adv.* **2018**, *8*, 34241–34251. [[CrossRef](#)]
16. Yayapao, O.; Thongtem, T.; Phuruangrat, A.; Thongtem, S. Synthesis and characterization of highly efficient Gd doped ZnO photocatalyst irradiated with ultraviolet and visible radiations. *Mater. Sci. Semicond. Process.* **2015**, *39*, 786–792. [[CrossRef](#)]
17. Das, A.; Kumar, P.M.; Bhagavathiachari, M.; Nair, R.G. Hierarchical ZnO-TiO₂ nanoheterojunction: A strategy driven approach to boost the photocatalytic performance through the synergy of improved surface area and interfacial charge transport. *Appl. Surf. Sci.* **2020**, *534*, 147321. [[CrossRef](#)]
18. Munguti, L.; Dejene, F. Effects of Zn:Ti molar ratios on the morphological, optical and photocatalytic properties of ZnO-TiO₂ nanocomposites for application in dye removal. *Mater. Sci. Semicond. Process.* **2021**, *128*, 105786. [[CrossRef](#)]
19. Suganthi, N.; Thangavel, S.; Kannan, K. Hibiscus subdariffa leaf extract mediated 2-D fern-like ZnO/TiO₂ hierarchical nanoleaf for photocatalytic degradation. *FlatChem* **2020**, *24*, 100197. [[CrossRef](#)]
20. Ali, M.M.; Haque, J.; Kabir, M.H.; Kaiyum, M.A.; Rahman, M. Nano synthesis of ZnO-TiO₂ composites by sol-gel method and evaluation of their antibacterial, optical and photocatalytic activities. *Results Mater.* **2021**, *11*, 100199. [[CrossRef](#)]
21. Shirsath, S.; Pinjari, D.; Gogate, P.; Sonawane, S.; Pandit, A. Ultrasound assisted synthesis of doped TiO₂ nano-particles: Characterization and comparison of effectiveness for photocatalytic oxidation of dyestuff effluent. *Ultrason. Sonochemistry* **2013**, *20*, 277–286. [[CrossRef](#)] [[PubMed](#)]
22. Pragathiswaran, C.; Smitha, C.; Abubakkar, B.M.; Govindhan, P.; Krishnan, N.A. Synthesis and characterization of TiO₂/ZnO-Ag nanocomposite for photocatalytic degradation of dyes and anti-microbial activity. *Mater. Today Proc.* **2021**, *45*, 3357–3364. [[CrossRef](#)]
23. Van Viet, P.; Vinh, T.H.T.; Dung, N.T.N.; Thi, C.M. Facile ball-milling synthesis of TiO₂ modified ZnO for efficient photocatalytic removal of atmospheric nitric oxide gas under solar light irradiation. *Chem. Phys. Lett.* **2021**, *775*, 138642. [[CrossRef](#)]
24. Hosseini, A.; Karimi, H.; Foroughi, J.; Sabzehmeidani, M.M.; Ghaedi, M. Heterogeneous photoelectro-Fenton using ZnO and TiO₂ thin film as photocatalyst for photocatalytic degradation Malachite Green. *Appl. Surf. Sci. Adv.* **2021**, *6*, 100126. [[CrossRef](#)]
25. Quang, T.; Viet, Q.; Hoang, V.; Thi, N.; Giang, H. Statistical screening and optimization of photocatalytic degradation of methylene blue by ZnO-TiO₂/rGO nanocomposite. *Colloids Surf. A Physicochem. Eng. Asp.* **2021**, *629*, 127464.
26. Khaki, M.R.D.; Shafeeyan, M.S.; Raman, A.A.A.; Daud, W.M.A.W. Evaluating the efficiency of nano-sized Cu doped TiO₂/ZnO photocatalyst under visible light irradiation. *J. Mol. Liq.* **2018**, *258*, 354–365. [[CrossRef](#)]
27. Huerta-Aguilar, C.A.; Palos-Barba, V.; Thangarasu, P.; Koodali, R.T. Visible light driven photo-degradation of Congo red by TiO₂ZnO/Ag: DFT approach on synergetic effect on band gap energy. *Chemosphere* **2018**, *213*, 481–497. [[CrossRef](#)]
28. Hou, T.; Chen, L.; Xin, Y.; Zhu, W.; Zhang, C.; Zhang, W.; Liang, S.; Wang, L. Porous CuFe for Plasmon-Assisted N₂ Photofixation. *ACS Energy Lett.* **2020**, *5*, 2444–2451. [[CrossRef](#)]
29. Nie, J.; Patrocínio, A.O.T.; Hamid, S.; Sieland, F.; Sann, J.; Xia, S.; Bahnemann, D.W.; Schneider, J. New insights into the plasmonic enhancement for photocatalytic H₂ production by Cu-TiO₂ upon visible light illumination. *Phys. Chem. Chem. Phys.* **2018**, *20*, 5264–5273. [[CrossRef](#)]
30. Potdar, S.B.; Praveen, B.; Sonawane, S.H. Sonochemical approach for synthesis of zinc oxide-poly methyl methacrylate hybrid nanoparticles and its application in corrosion inhibition. *Ultrason. Sonochemistry* **2020**, *68*, 105200. [[CrossRef](#)]
31. Khan, A.; Rashid, A.; Younas, R.; Chong, R. A chemical reduction approach to the synthesis of copper nanoparticles. *Int. Nano Lett.* **2016**, *6*, 21–26. [[CrossRef](#)]
32. An, M.; Li, L.; Wu, Q.; Yu, H.; Gao, X.; Zu, W.; Guan, J.; Yu, Y. CdS QDs modified three-dimensional ordered hollow spherical ZnTiO₃-ZnO-TiO₂ composite with improved photocatalytic performance. *J. Alloy Compd.* **2021**, *895*, 162638. [[CrossRef](#)]
33. Potdar, S.B.; Huang, C.-M.; Praveen, B.; Manickam, S.; Sonawane, S.H. Highly Photoactive Titanium Dioxide Supported Platinum Catalyst: Synthesis Using Cleaner Ultrasound Approach. *Catalysts* **2022**, *12*, 78. [[CrossRef](#)]
34. Chen, B.; Zhang, J.; Yu, J.; He, B.; Jin, J.; Wang, H.; Gong, Y. Rational design of all-solid-state TiO_{2-x}/Cu/ZnO Z-scheme heterojunction via ALD-assistance for enhanced photocatalytic activity. *J. Colloid Interface Sci.* **2022**, *607*, 760–768. [[CrossRef](#)] [[PubMed](#)]
35. Mohammed, A.M.; Mohtar, S.S.; Aziz, F.; Aziz, M.; Ul-Hamid, A.; Salleh, W.N.W.; Yusof, N.; Jaafar, J.; Ismail, A.F. Ultrafast degradation of Congo Red dye using a facile one-pot solvothermal synthesis of cuprous oxide/titanium dioxide and cuprous oxide/zinc oxide p-n heterojunction photocatalyst. *Mater. Sci. Semicond. Process.* **2021**, *122*, 105481. [[CrossRef](#)]
36. Joseph, P.D.; Venkateswaran, C. Bandgap engineering in ZnO by doping with 3d transition metal ions. *J. At. Mol. Physics.* **2011**, *2011*, 270540. [[CrossRef](#)]

37. Magdalane, C.M.; Priyadharsini, G.M.A.; Kaviyarasu, K.; Jothi, A.I.; Simiyon, G.G. Synthesis and characterization of TiO₂ doped cobalt ferrite nanoparticles via microwave method: Investigation of photocatalytic performance of congo red degradation dye. *Surf. Interfaces* **2021**, *25*, 101296. [[CrossRef](#)]
38. Yang, Y.; Ali, N.; Khan, A.; Khan, S.; Khan, S.; Khan, H.; Xiaoqi, S.; Ahmad, W.; Uddin, S.; Ali, N.; et al. Chitosan-capped ternary metal selenide nanocatalysts for efficient degradation of Congo red dye in sunlight irradiation. *Int. J. Biol. Macromol.* **2021**, *167*, 169–181. [[CrossRef](#)]
39. Khan, S.; Khan, A.; Ali, N.; Ahmad, S.; Ahmad, W.; Malik, S.; Ali, N.; Khan, H.; Shah, S.; Bilal, M. Degradation of Congo red dye using ternary metal selenide-chitosan microspheres as robust and reusable catalysts. *Environ. Technol. Innov.* **2021**, *22*, 101402. [[CrossRef](#)]
40. Sarkar, C.; Basu, J.K.; Samanta, A.N. Synthesis of novel ZnO/Geopolymer nanocomposite photocatalyst for degradation of congo red dye under visible light. *Environ. Nanotechnol. Monit. Manag.* **2021**, *16*, 100521. [[CrossRef](#)]
41. Shekardasht, M.B.; Givianrad, M.H.; Gharbani, P.; Mirjafary, Z.; Mehrizad, A. Preparation of a novel Z-scheme g-C₃N₄/RGO/Bi₂Fe₄O₉ nanophotocatalyst for degradation of Congo Red dye under visible light. *Diam. Relat. Mater.* **2020**, *109*, 108008. [[CrossRef](#)]
42. Bhagwat, U.O.; Wu, J.J.; Asiri, A.M.; Anandan, S. Photocatalytic Degradation of Congo Red Using PbTiO₃ Nanorods Synthesized via a Sonochemical Approach. *ChemistrySelect* **2018**, *3*, 11851–11858. [[CrossRef](#)]
43. Ma, C.; Wang, F.; Zhang, C.; Yu, A.; Wei, J.; Yang, Z.; Li, Y.; Li, Z.; Zhu, M.; Shen, L.; et al. Photocatalytic decomposition of Congo red under visible light irradiation using MgZnCr-TiO₂ layered double hydroxide. *Chemosphere* **2017**, *168*, 80–90. [[CrossRef](#)]
44. Ljubas, D.; Smoljanić, G.; Juretić, H. Degradation of Methyl Orange and Congo Red dyes by using TiO₂ nanoparticles activated by the solar and the solar-like radiation. *J. Environ. Manag.* **2015**, *161*, 83–91. [[CrossRef](#)] [[PubMed](#)]
45. Sadollahkhani, A.; Ibupoto, Z.H.; Elhag, S.; Nur, O.; Willander, M. Photocatalytic properties of different morphologies of CuO for the degradation of Congo red organic dye. *Ceram. Int.* **2014**, *40*, 11311–11317. [[CrossRef](#)]
46. Khairol, N.F.; Sapawe, N.; Danish, M. Photocatalytic Study of ZnO-CuO/ES on Degradation of Congo Red. *Mater. Today Proc.* **2019**, *19*, 1333–1339. [[CrossRef](#)]
47. Yang, J.; Shi, C.; Dong, Y.; Su, H.; Sun, H.; Guo, Y.; Yin, S. Efficient hydrogen generation of vector Z-scheme CaTiO₃/Cu/TiO₂ photocatalyst assisted by cocatalyst Cu nanoparticles. *J. Colloid Interface Sci.* **2022**, *605*, 373–384. [[CrossRef](#)]